

# Bosonic $Z_2$ metal: Spontaneous breaking of time-reversal symmetry due to Cooper pairing in the resistive state of $\text{Ba}_{1-x}\text{K}_x\text{Fe}_2\text{As}_2$

Vadim Grinenko,<sup>1,2,\*</sup> Daniel Weston,<sup>3</sup> Federico Caglieris,<sup>2</sup> Christoph Wuttke,<sup>2</sup> Christian Hess,<sup>2,4</sup> Tino Gottschall,<sup>5</sup> Jochen Wosnitza,<sup>1,5</sup> Andreas Rydh,<sup>6</sup> Kunihiro Kihou,<sup>7</sup> Chul-Ho Lee,<sup>7</sup> Rajib Sarkar,<sup>1</sup> Shanu Dengre,<sup>1</sup> Ilaria Maccari,<sup>3</sup> Julien Garaud,<sup>8</sup> Aliaksei Charnukha,<sup>2</sup> Ruben Hühne,<sup>2</sup> Kornelius Nielsch,<sup>2</sup> Bernd Büchner,<sup>1,2</sup> Hans-Henning Klauss,<sup>1</sup> and Egor Babaev<sup>3,†</sup>

<sup>1</sup>*Institute for Solid State and Materials Physics,  
Technische Universität Dresden, 01069 Dresden, Germany*

<sup>2</sup>*Leibniz IFW Dresden, 01067 Dresden, Germany*

<sup>3</sup>*Department of Physics, KTH Royal Institute of Technology, SE-106 91 Stockholm, Sweden*

<sup>4</sup>*Fakultät für Mathematik und Naturwissenschaften,  
Bergische Universität Wuppertal, 42097 Wuppertal, Germany*

<sup>5</sup>*Dresden High Magnetic Field Laboratory (HLD-EMFL) and Würzburg-Dresden Cluster  
of Excellence st.qmat Helmholtz-Zentrum Dresden-Rossendorf, 01328 Dresden, Germany*

<sup>6</sup>*Department of Physics, Stockholm University, SE-106 91 Stockholm, Sweden*

<sup>7</sup>*National Institute of Advanced Industrial Science and  
Technology (AIST), Tsukuba, Ibaraki 305-8568, Japan*

<sup>8</sup>*Institut Denis Poisson CNRS-UMR 7013, Université de Tours, 37200 France*

Superconductivity is described by an order parameter of second order (i.e. quadratic) in fermionic fields, representing electrons forming pairs. However, in systems with electronic pairing instabilities in several bands there might exist a phase that is different by symmetry from both normal metal and superconductor. This non-superconducting state is described by an order parameter that is of fourth order in fermionic fields. Here, we report the observation of such a phase in the superconductor  $\text{Ba}_{1-x}\text{K}_x\text{Fe}_2\text{As}_2$ . This novel state can be characterized as a bosonic  $Z_2$  metal, which spontaneously breaks time-reversal symmetry as a consequence of the formation of non-condensed Cooper-pairs. In this state, the phases of the gaps in different bands are disordered and superconductivity is absent. However, the gaps do not fluctuate independently and

there is a broken time-reversal symmetry due to a non-trivial difference between the fluctuating phases in different bands. Hence, this state can be described as an ordering which is fourth order in fermions, i.e. consists of correlations between pairs of noncondensed Cooper pairs of fermions in different bands. When temperature is decreased, the system undergoes a superconducting phase transition and enters a  $U(1) \times Z_2$  superconducting state. This is in precise agreement with earlier muon spin rotation experiments on the formation of  $s + is$  or  $s + id$  superconducting states at low temperatures in  $Ba_{1-x}K_xFe_2As_2$  for the present doping. We demonstrate that a bosonic  $Z_2$  metal shows a number of novel physical properties.

## INTRODUCTION

The Bardeen-Cooper-Schrieffer (BCS) [1, 2] and Ginzburg-Landau [3] theories describe a superconducting state of matter arising via a single phase transition. In the weak-coupling mean-field BCS theory the phase transition separates a fermionic normal state from a bosonic superconducting state described by a classical field, which is proportional to the complex gap function  $\Delta$ . Going beyond the mean-field theory, weak coupling leads to the existence of Cooper-pairing fluctuations above the critical temperature [4], while at stronger coupling no fermionic pairbreaking occurs at the phase transition [5–7]. Unless a superconductor is strongly type I, in this case the phase transition is driven by topologically nontrivial phase fluctuations [8, 9]. In zero external field these fluctuations are described as proliferation of vortex loops, whereas in finite fields they are characterized as vortex lattice melting [8–12]. Although this implies that the normal state just above the phase transition is in general bosonic, this does not constitute a different phase since it is not distinguished by symmetry from a purely fermionic state. Rather, with increased temperature the bosonic correlations gradually vanish without a phase transition.

However, in a multicomponent superconductor there might exist a non-superconducting state with preformed pairs which differs by symmetry from the normal state. This situation can arise in multiband superconductors with a multicomponent order parameter having the form  $k_1 + ik_2$ , where  $k_j = s$  or  $d$ . Such states are a consequence of the presence of several gaps in multiband materials. When the interactions between bands are frustrated, an additional  $Z_2$  double-degeneracy of the ground state can appear. This occurs, when phase differences between gaps in different bands have values other than 0 or  $\pi$  [13–16]. Such a state spontaneously breaks time-reversal symmetry

since complex conjugation of the gaps puts one in a different ground state. At the level of mean-field theory, the  $U(1)$  symmetry is broken at a higher temperature  $T_c^{U(1)}$  than the temperature  $T_c^{Z_2}$  at which the time-reversal  $Z_2$  symmetry is broken. Within these models one does not obtain  $T_c^{U(1)} < T_c^{Z_2}$  and for  $s+is$  and  $s+id$  states it is in general difficult to obtain degenerate temperatures  $T_c^{U(1)} = T_c^{Z_2}$  [13–17]. Therefore, a phase diagram as a function of doping at mean-field level generically looks like a dome of  $k_1 + ik_2$  state between two superconducting states having  $k_1$  and  $k_2$  order parameters, where the maximal  $T_c^{Z_2}$  does not touch  $T_c^{U(1)}$  (Fig. 1a).

The situation is different, if one goes beyond mean-field approximation in such systems. Fluctuation effects have been considered in the London model of  $s + is$  superconductors, and it was found that in two as well as three spatial dimensions a situation can arise where  $T_c^{U(1)} < T_c^{Z_2}$  [18, 19]. In three dimensions the occurrence of this phase depends on the parameters of the model, and in particular on the value of the magnetic-field penetration length relative to the other length scales. The fact that  $T_c^{U(1)} < T_c^{Z_2}$  implies a novel bosonic metallic state, where time-reversal symmetry is spontaneously broken. This state is related to the metallic superfluid phase discussed in the context of metallic hydrogen [20, 21], with the principle difference that here the interband coupling only allows the breaking of a discrete  $Z_2$  symmetry. The novel bosonic metallic state is separated from the normal state by another phase transition at which time-reversal symmetry is restored. Therefore, beyond mean-field approximation the line of  $T_c^{Z_2}$  as a function of doping can go above the line of  $T_c^{U(1)}$  in the phase diagram of materials such as  $Ba_{1-x}K_xFe_2As_2$  (Fig.1b). Experimentally, the phase transition at  $T_c^{Z_2}$  manifests itself as follows: When  $T_c^{U(1)} > T_c^{Z_2}$  the jump in specific heat should coincide with the superconducting phase transition. If at certain doping one gets  $T_c^{U(1)} < T_c^{Z_2}$ , the specific-heat jump will occur above the temperature of the superconducting response. For a realistic system with some inhomogeneities, this behavior would be diametrically opposite to the usual behavior, where the system typically starts showing some diamagnetic response before the superconducting transition reveals itself in the specific heat jump, since often superconductivity occurs non-uniformly in an imperfect sample.

The long sought-after  $s + is$  state, in which time-reversal symmetry is broken as a result of frustration between Josephson-coupled superconducting bands, has been predicted theoretically in  $Ba_{1-x}K_xFe_2As_2$  [13–16]. Recent experimental indications of such an  $s + is$  state in this material were obtained in muon spin rotation ( $\mu$ SR) experiments [22, 23], which were focused primarily on low-temperature states. Here, we conduct combined calorimetry, magnetization and transport

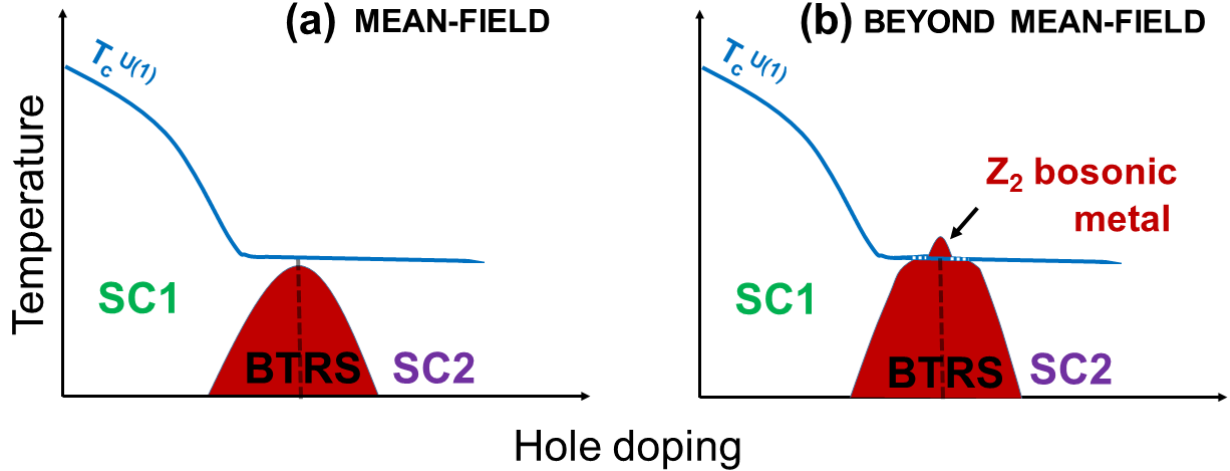


FIG. 1: **Schematic phase diagram.** (a) The extended superconducting dome with two different  $s_{\pm}$  states is separated by an intermediate state with a complex  $s + is$  order parameter that breaks time-reversal symmetry. According to mean-field theory the BTRS dome is usually located below the  $T_c^{U(1)}$  line and cannot go above  $T_c^{U(1)}$ . (b) The corresponding schematic phase diagram expected in the case when superconducting fluctuations are taken into account [18, 19]. Fluctuations suppress  $T_c^{U(1)}$  more than  $T_c^{Z_2}$ . Above  $T_c^{U(1)}$ , Cooper pairs are formed without global phase coherence, when the system is not superconducting. The breaking of time-reversal symmetry in the normal state is driven by interband interactions that lock the relative phases between fluctuating Cooper pairs in different bands.

measurements, and show that in contrast to mean-field predictions  $\text{Ba}_{1-x}\text{K}_x\text{Fe}_2\text{As}_2$  has a novel type of metallic state of matter, characterized by an order parameter which is fourth order in fermionic fields.

To study the properties of the BTRS superconducting state, we select  $\text{Ba}_{1-x}\text{K}_x\text{Fe}_2\text{As}_2$  single crystals with  $0.65 \lesssim x \lesssim 0.85$ , covering a region in the phase diagram with two different  $s_{\pm}$  and intermediate  $s + is$  states. All crystals were examined by x-ray diffraction and the doping level was defined using the known dependence of the  $c$ -axis on K doping [24]. The investigated single crystals were thin plates with an area of several  $\text{mm}^2$  and a thickness of 5 - 50  $\mu\text{m}$ . The crystals show high residual resistivity ratios  $\text{RRR} = \rho_{300\text{K}}/\rho_0 \sim 100$  (see the supplementary material). The zero-field specific heat together with the low-field static magnetic susceptibility close to  $T_c$  is shown in Fig. 2 for  $\text{Ba}_{1-x}\text{K}_x\text{Fe}_2\text{As}_2$  single crystals with different doping levels. Panels (a) and (b) show data from crystals with  $s_{\pm 1}$  state that preserves time-reversal symmetry. In this state, the order parameter changes sign between electron and hole Fermi pockets [25]. This results in the fact that all hole pockets having the same sign of the order parameter. Panel (h) covers the doping region of the  $s_{\pm 2}$  state, which also preserves time-reversal symmetry. In this case it is

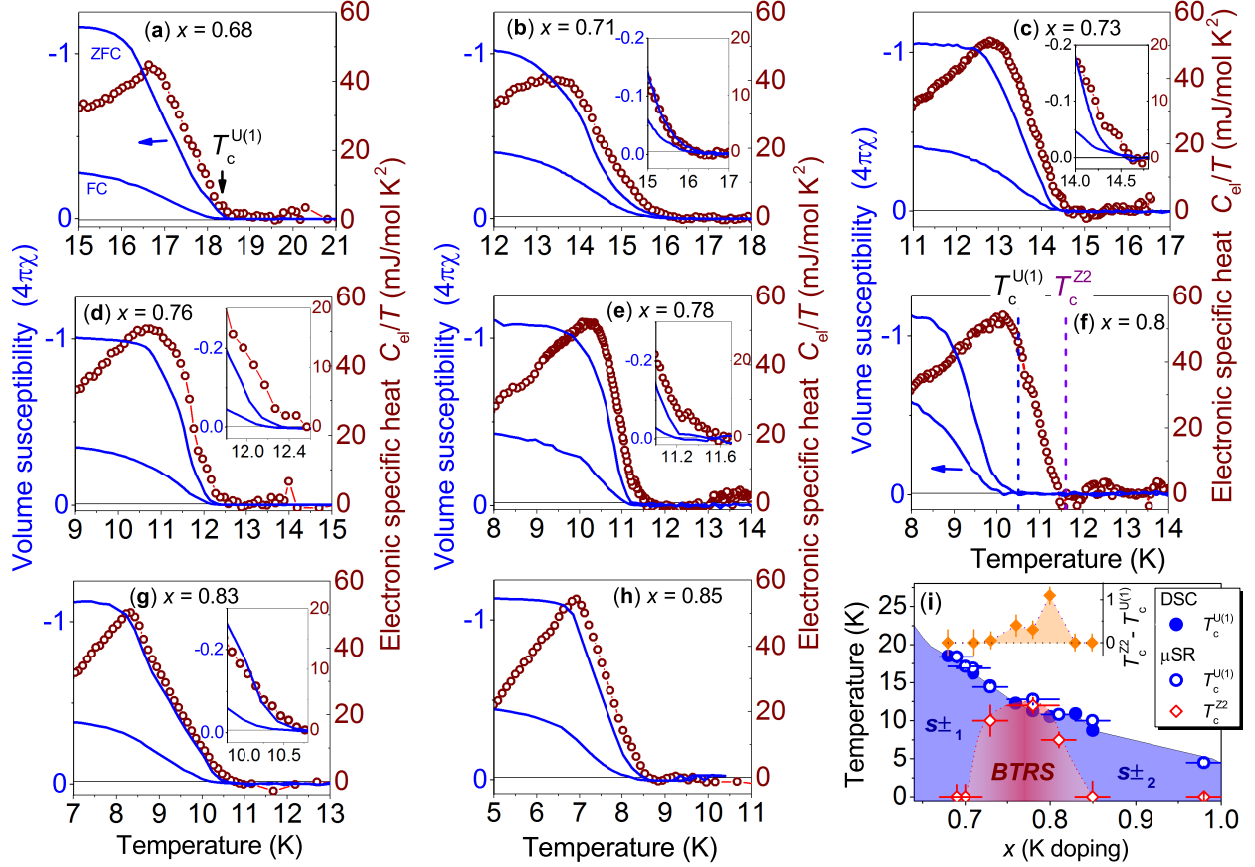


FIG. 2:  $\text{Ba}_{1-x}\text{K}_x\text{Fe}_2\text{As}_2$  at different doping levels  $x$  (a) - (h) Temperature dependence of magnetic susceptibility (left axis) and the zero field specific heat (right axis) close to the superconducting transition temperature  $T_c^{U(1)}$  for samples with different K doping level  $x$ . The figures show splitting of two phase transitions and the appearance of a  $Z_2$  phase at  $T_c^{U(1)} < T_c^{Z_2}$ . (i) Experimental phase diagram constructed using the susceptibility and specific-heat data (closed symbols), and data taken from Refs. [22, 23] (open symbols). Panels (a) and (b) refer to samples from the  $s_{\pm 1}$  region on the phase diagram, panels (c) - (f) refer to samples within the BTRS dome, and panels (g) and (h) refer to samples from the  $s_{\pm 2}$  region.

expected that the order parameter changes sign between hole Fermi pockets in the zone center [25]. Data from samples with the intermediate  $s + is$  state are shown in panels (c)-(g). In both  $s_{\pm}$  superconducting states the combined calorimetry and magnetization measurements give the standard picture of a superconducting phase transition, namely that the onset of the anomaly in the specific heat coincides with the onset of the diamagnetic signal in the susceptibility. However, close to the summit of the  $s + is$  dome the onset temperature seen in the specific heat splits apart from the onset temperature seen in the susceptibility. The splitting is especially pronounced for the sample that corresponds to the summit of the BTRS dome (panels (f) and (i)), i.e. at the maximal critical temperature  $T_c^{Z_2}$ . Close to the summit, the breaking of time-reversal symmetry

is strongest, and thus the energy cost of  $Z_2$  domain walls is highest. Therefore, the splitting of  $T_c^{Z_2}$  and  $T_c^{U(1)}$  should also be maximal. Importantly, when the specific heat jump splits from the transition seen in susceptibility and resistivity (Fig. 3), it leaves no resolvable thermodynamic features at the lower transition. The dominance of the  $Z_2$  transition in calorimetric signatures for the regime  $T_c^{Z_2} > T_c^{U(1)}$  is also in agreement with the numerical simulations we performed, which will be discussed below.

Next we discuss the characterization of the new metallic state that spontaneously breaks time-reversal symmetry due to bosonic fluctuations, and which we find at  $T_c^{Z_2} > T > T_c^{U(1)}$ . The physical properties of the sample with  $x = 0.8$ , showing the largest splitting between the transitions, are summarized in Fig. 3. Panel (a) shows the temperature dependence of the electrical resistivity measured at different transport currents. The resistivity deviates from the normal-state behavior and obeys a current dependence below the crossover temperature  $T^*$ . In addition, we found that  $T_c^{U(1)}$  defined from the AC susceptibility depends on the frequency of the applied AC magnetic field (see panel (b)). Both of these current and frequency dependent properties above the zero-resistance state indicate the presence of pairing fluctuations above the bulk  $T_c^{U(1)}$ , at which the resistance is zero. However, the jump in specific heat is observed in the intermediate temperature range between  $T^*$  and  $T_c^{U(1)}$ . To verify the nature of this transition we perform nuclear quadrupole resonance (NQR) measurements summarized in panel (c). We did not find any noticeable increase of the spin-lattice relaxation rate  $1/T_1$  or the width and shape of the NQR line across  $T_c^{U(1)}$ . This makes it improbable that the phase transition at  $T_c^{Z_2}$  is related to some sort of magnetism, charge or nematic order. In addition, in the case of coexisting/competing orders with superconductivity one expects a second specific heat jump at  $T_c^{U(1)}$  comparable to the specific heat jumps at the superconducting transitions at other dopings. By contrast, for fluctuation-induced phases such as the bosonic  $Z_2$  metal the mean-field-like feature in specific heat will be dominated by the  $Z_2$  transition. Since the anomaly at  $T_c^{U(1)}$  can hardly be seen in our data, we conclude that the transition at  $T_c^{Z_2}$  must be related to the existence of Cooper pairs. The specific heat down to  $T \sim 0.4$  K is shown in the panel (d). The mean-field features in the specific heat are quite similar to the superconducting transition except that for this doping the jump occurs above  $T_c^{U(1)}$ . The corresponding mean-field estimate shows that the entropy related to the transition at  $T_c^{Z_2}$  can be fully accounted for by a state with Cooper pairing. In panel (d) we also show the muon spin relaxation rate taken from Ref. [23] for the sample with  $x = 0.78(3)$  having the strongest BTRS signal. The crystal studied in this work was a part of this sample used for  $\mu$ SR measurements.

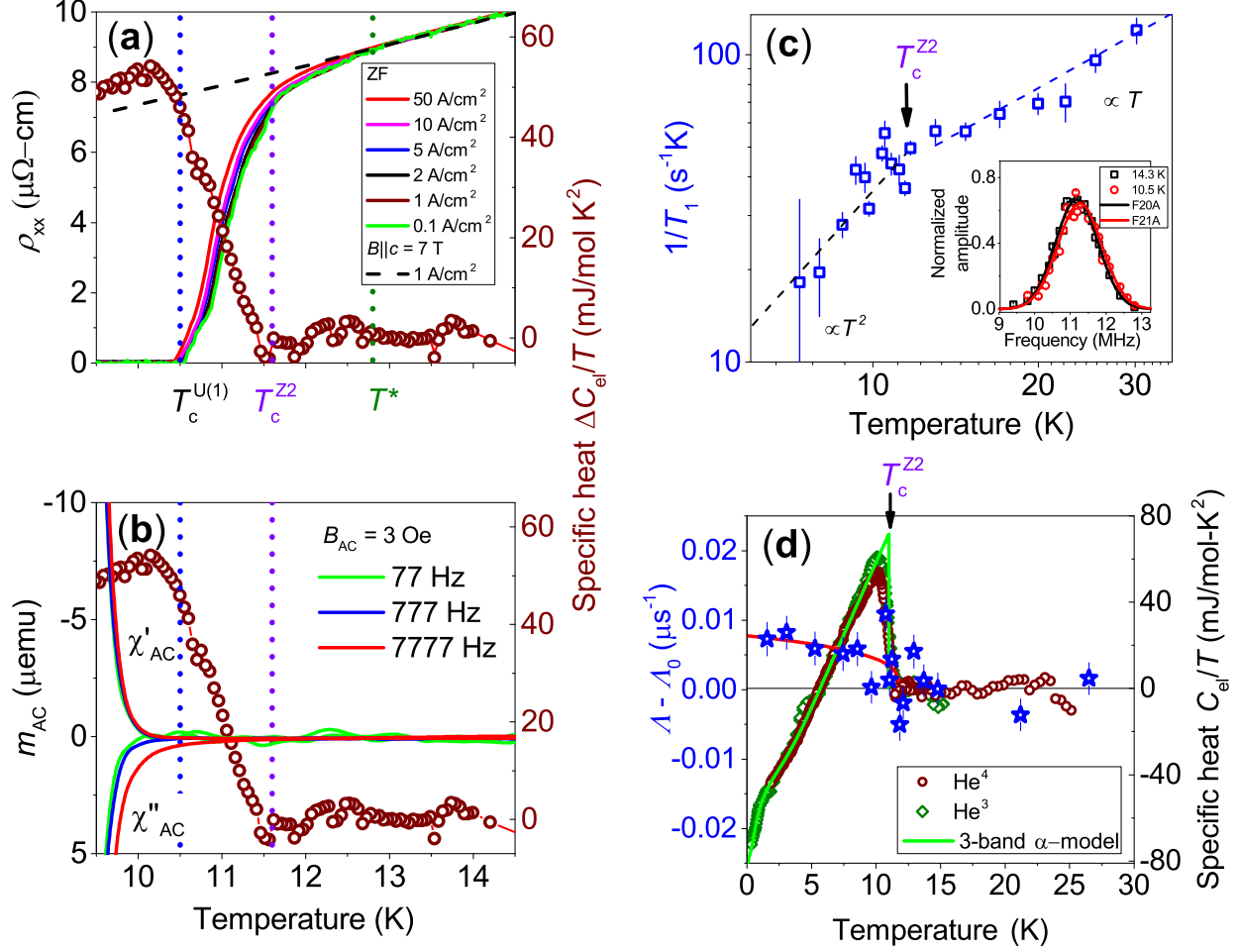


FIG. 3: **Low-temperature physical properties of the sample with  $x = 0.8$**  (a) Temperature dependence of the longitudinal electrical resistivity measured at different AC transport current amplitudes with the frequency 173 Hz (left axis) compared with the temperature dependence of the zero-field specific heat (right axis). (b) Temperature dependence of the AC susceptibility measured at different frequencies (left axis) compared with the temperature dependence of the zero-field specific heat (right axis). (c) Temperature dependence of the NQR spin-lattice relaxation rate  $1/T_1$ ; the inset shows NQR spectra in the normal state and in the  $Z_2$  metal phase. We found that both the  $1/T_1$  and the width of the spectra are not enhanced across  $T_c^{Z_2}$ . (d) Temperature dependence of the muon spin relaxation rate (left axis) and the electronic specific heat measured down to 0.4 K (right axis). At the level of mean-field analysis the entropy is conserved, indicating an electronic origin of the transition at  $T_c^{Z_2}$ . The  $\mu\text{SR}$  data are taken from Ref. [23] for the sample with  $x = 0.78(3)$ .

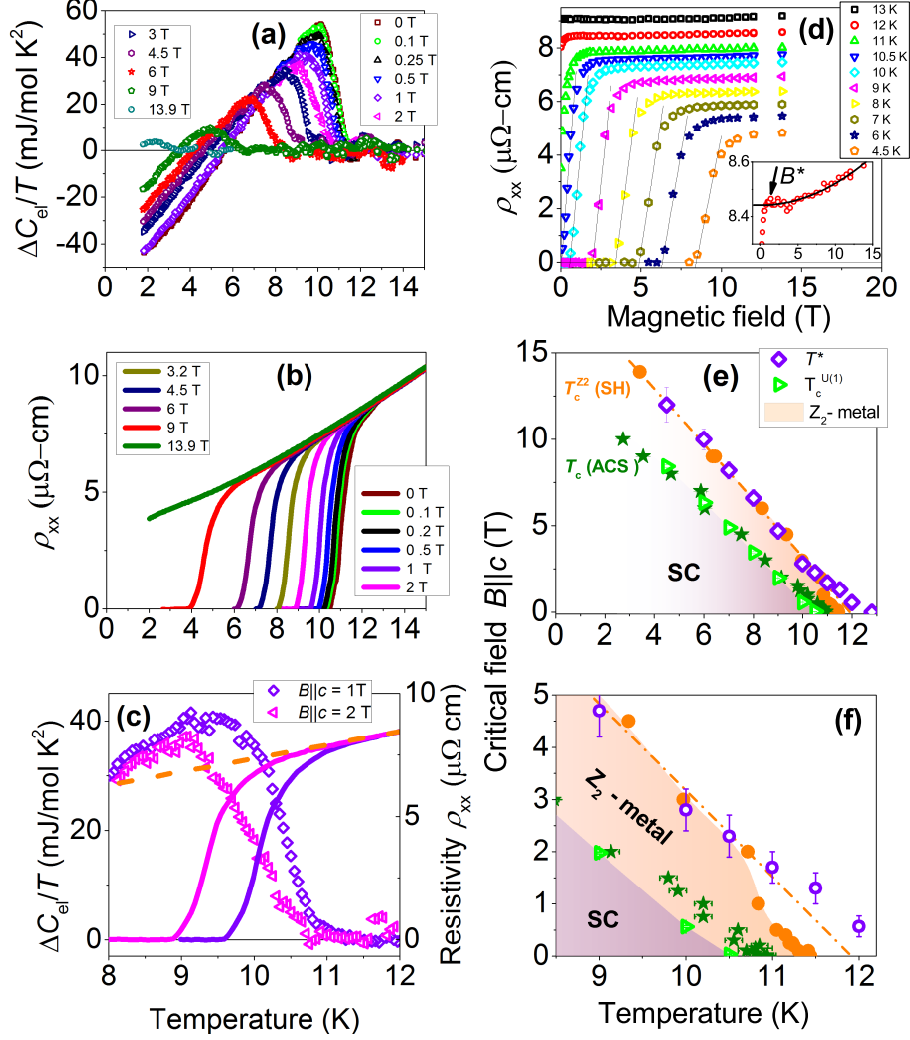


FIG. 4: **In-field properties of the sample with  $x = 0.8$**  (a) Temperature dependence of the specific heat. (b) Temperature dependence of the longitudinal electrical resistivity measured with the AC current amplitude 1 A/cm<sup>2</sup> and the frequency 173 Hz. (c) Temperature dependence of the specific heat (left axis, symbols) compared with the temperature dependence of the resistivity (right axis, lines) for  $B||c = 1$  T and 2 T. The dashed line is the resistivity data for  $B||c = 7$  T. The superconducting transition temperature measured by the resistivity is more sensitive to magnetic field as compared to the anomaly in the specific heat. (d) Magnetoresistance at different temperatures. Strong magnetoresistance is observed below  $B^*$ , which is attributed to the crossover field for the pairing fluctuations. Inset shows magnetoresistance at  $T = 12$  K. (e) Experimental magnetic-field phase diagram. The region with the bosonic  $Z_2$ -metal state is colored. The relative splitting between the critical temperatures is increased in increased field. (f) The low-field region of the same phase diagram as in panel (e).



Important insight into the properties of the transition at  $T_c^{Z_2}$  can be obtained by studying the phase diagram as a function of applied magnetic field. The temperature dependencies of the specific heat and the electrical resistivity  $\rho_{xx}$  of the sample with  $x = 0.8$  for different magnetic fields applied along the  $c$ -axis are shown in Fig. 4a and Fig. 4b. Both the temperature of the specific-heat anomaly and the superconducting transition temperature in the electrical transport are monotonically suppressed by magnetic field, i.e. shifted to lower temperatures. However, the suppression rate is quite different. In the highest measured magnetic field of about 14 T the specific heat jump is well resolved but the resistivity obeys nearly a normal state behaviour with only a weak feature across the anomaly in the specific heat. The difference in the suppression rates of  $T_c^{Z_2}$  and  $T_c^{U(1)}$  is especially pronounced in the low field range. An increase of the field from 1 T to 2 T only slightly affects the specific heat but strongly shifts the superconducting transition seen in the resistivity (Fig.4d). The well-resolvable specific heat jump in external field is again consistent with the  $Z_2$  metal phase. This is because the  $Z_2$ -metal-to-normal phase transition is driven by the proliferation of domain walls in phase differences. The field-induced vortices do not directly contribute to the  $Z_2$  phase transition; their role is secondary and arises from their interaction with domain walls, which is a non-linear effect [26, 27].

Further insight into the properties of the fluctuating state at  $T_c^{U(1)} < T < T^*$  is obtained from the field dependence of the electrical resistivity at constant temperature (Fig.4c). In the normal state, the magnetoresistance  $\rho_{xx}(B) \propto B^2$  is small ( $\sim 1\%$  in  $B = 14$  T applied along the  $c$ -axis). At  $T \lesssim 12.5$  K and below the threshold field  $B^*$ , the magnetoresistance changes behavior, i.e. approaches zero linearly (Fig.4d). The linear magnetoresistance is expected in the flux-flow regime [28]. In this state, the vortex system is in the liquid state and a superconductor behaves as a normal metal. The U(1) symmetry is preserved since the phase of the superconducting order parameter is disordered [8–12]. We discuss this in more detail below, in the section on the theoretical analysis. The linear infield behaviour of the magnetoresistance allows one to obtain the field dependence of the bulk superconducting critical temperature  $T_c^{U(1)}$  using a linear approximation as shown in Fig. 4d. The obtained values of  $T_c^{U(1)}$  agree with the critical temperature defined by the splitting between the real and imaginary parts of the AC susceptibility (for AC susceptibility data see the supplementary material). The obtained field dependencies of the characteristic temperatures are summarized in Fig. 4e and Fig. 4f. It is seen that the overall temperature scale of the phase diagram is given by the onset of superconducting fluctuations at  $T^*$ . The phase transition seen in the specific heat at  $T_c^{Z_2}$  is observed below  $T^*$  in low magnetic fields and is limited by  $T^*$  above

$B \sim 2$  T. This behaviour is consistent with our main statement that  $T_c^{Z_2}$  is related to pairing correlations, and thus cannot exceed  $T^*$ .

### Theoretical analysis

At the level of mean-field theory the superconducting phase transition always occurs at a temperature equal to or higher than the BTRS transition temperature. However, if fluctuations are included, an anomalous  $Z_2$ -metal phase can occur in which time-reversal symmetry is broken but superconducting order is absent, at least in a lattice version of the model we consider. This has been shown previously in a London model in both two and three spatial dimensions [18, 19]. In the related London model for three dimensions, the  $Z_2$  metal phase occurs for relatively large values of the coupling constant, corresponding to relatively short penetration depths. This, along with the fact that experimentally the splitting of  $T_c^{Z_2}$  and  $T_c^{U(1)}$  is relatively small, requires an analysis that includes fluctuations of the density field. Ginzburg-Landau models for such systems have been derived microscopically, see e.g. Refs. [15, 29]. However, quantitative certainty about the form of the Ginzburg-Landau model requires much deeper insight into the microscopic physics of the material, which is currently unknown. We therefore include amplitude fluctuations in the rather generic BTRS form of the Ginzburg-Landau model consistent with Refs. [15, 29], and use the experimental observations to put constraints on it (further details can be found in the supplementary material).

We consider the Ginzburg-Landau model for a clean three-band superconductor in three spatial dimensions given by the free-energy density

$$f = \frac{1}{2}(\nabla \times \mathbf{A})^2 + \sum_i \frac{1}{2}|(\nabla + ie\mathbf{A})\psi_i|^2 + a_i|\psi_i|^2 + \frac{b_i}{2}|\psi_i|^4 + \sum_{i<j} \eta_{ij}|\psi_i||\psi_j| \cos(\phi_i - \phi_j), \quad (1)$$

which has been argued to describe the material in question [15, 29]. Here  $\mathbf{A}$  is the magnetic vector potential and  $\psi_i = |\psi_i|e^{i\phi_i}$  are matter fields corresponding to the superconducting components. There is also a reduced version of this model with only two components but a higher-order Josephson coupling; our conclusions will apply to this case as well. Note however that the derivation of the Ginzburg-Landau functional (1) neglects some terms, such as for example Andreev-Bashkin gradient terms coming from Fermi-liquid corrections or strong correlations. These terms play an important role for the existence and size of the  $Z_2$  metal state.

Apart from terms present in an ordinary single-component Ginzburg-Landau model, we have

Josephson-coupling terms that directly couple the three components. Depending on the sign of the coefficient  $\eta_{ij}$ , a Josephson term will be minimized, when the corresponding phase difference is either 0 or  $\pi$ . For some combinations of signs of the coefficients  $\eta_{ij}$ , it is impossible to simultaneously minimize each term, and in these cases the system is frustrated. If this phase frustration is strong enough, the ground state will be such that the phase differences between components are not all 0 or  $\pi$ . This defines  $s + is$  superconductivity where time-reversal symmetry is broken [13–15]. There are four combinations of signs of the coefficients  $\eta_{ij}$ : two equivalent combinations that give rise to phase frustration and two equivalent combinations that do not. (The equivalence consists of switching the sign of the couplings related to a certain phase and adding  $\pi$  to this phase.) For definiteness and without loss of generality we consider the case when each Josephson coupling is repulsive, meaning that all phase differences tend to be equal to  $\pi$ . Since a  $Z_2$  symmetry is broken when the phase differences are not all equal to 0 or  $\pi$ , we can define a  $Z_2$  Ising order parameter  $m$ . We define  $m$  to be equal to +1 for one of the chiralities of the phases and equal to  $-1$  for the other chirality (Fig. 5). In other words, the field  $m(\mathbf{r})$  takes the value +1 at points, where the phases are ordered 1, 2, 3 and takes the value  $-1$  at points where, the phases are ordered 1, 3, 2. When the  $Z_2$  symmetry is broken, the spatial average  $m$  of the field  $m(\mathbf{r})$  will be nonzero.

Since in the measurements the magnetic field is not completely screened, we also consider nonzero external magnetic field. This is particularly important as the area of interest is very close to the critical temperature, whence in the cooling process even a small magnetic field will exceed the first critical magnetic field  $H_{c1}$  for some temperature range. However, first we assess the limit of zero external field. In that limit we begin by considering the parameter values that are most favorable to the occurrence of the  $Z_2$ -metal phase in the class of models (1). That is, we consider the conditions where the spontaneous breaking of the  $Z_2$  symmetry is the strongest in this class of models. The  $Z_2$  symmetry is restored when domain walls proliferate, and the  $U(1)$  symmetry is restored when vortices proliferate. Thus, we want domain walls to be as energetically expensive as possible, relative to vortices (see the derivation in the supplementary material). Assuming that the superconductor is type II near the superconducting phase transition, we find that there is no fluctuation-induced  $Z_2$  metal phase in *exactly* zero external magnetic field for superconductors described by the model (1). However, the superconducting phase transition can be split from the phase transition associated with order in the phase differences between components when even a weak external field is applied, as has been discussed previously in London models [20, 21, 30]. We find that beyond the London limit, the  $Z_2$  metal phase appears in the type II regime in the

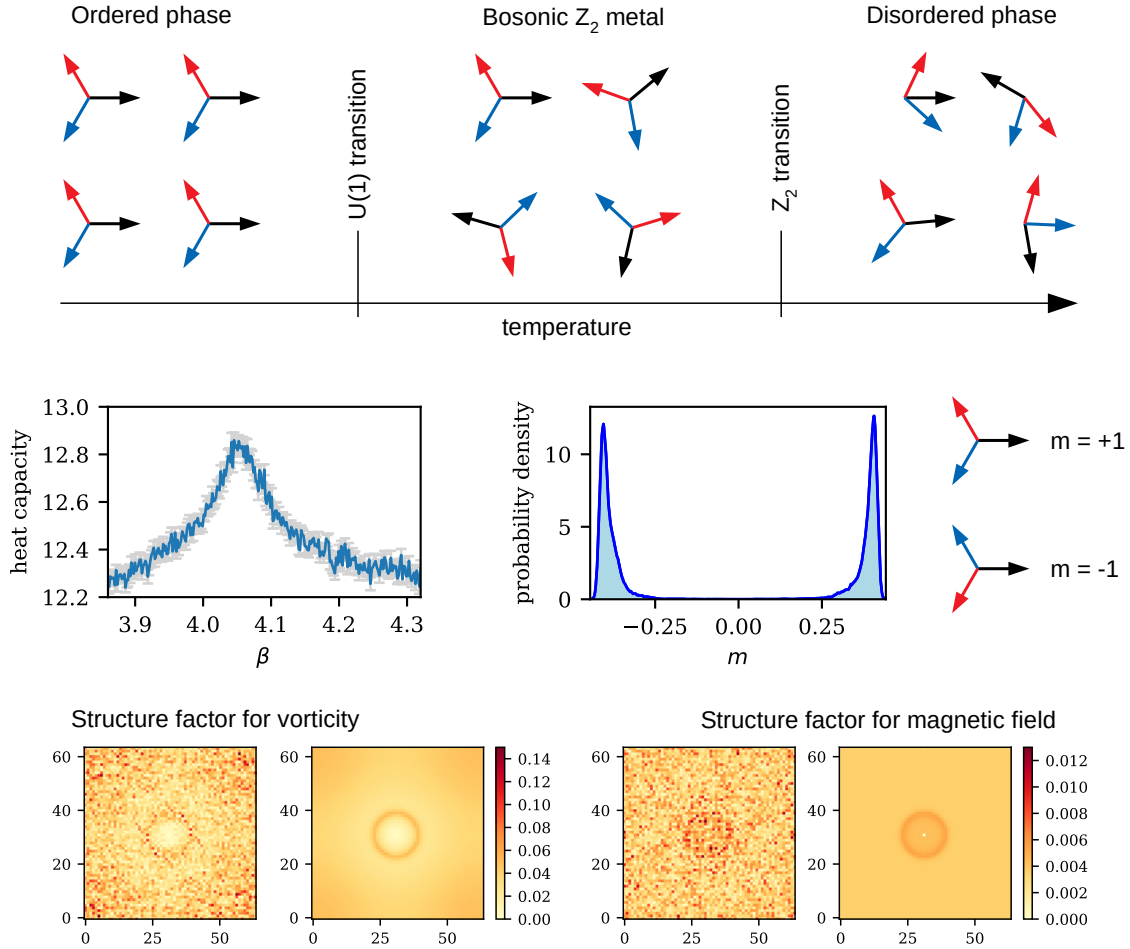


FIG. 5: **Three-component Ginzburg-Landau model.** **Top row:** Schematic illustration of the three phases: fully ordered, bosonic  $Z_2$  metal, and fully disordered. In the fully ordered phase, the system is superconducting and spontaneously breaks  $U(1) \times Z_2$  symmetry. In the bosonic  $Z_2$ -metal phase, the system is non-superconducting and spontaneously breaks only  $Z_2$  symmetry. **Middle row:** Heat capacity  $L^{-3} d\langle E \rangle / dT$  versus inverse temperature  $\beta = T^{-1}$  for the system with applied field that we consider. (Parameters are given in the supplementary material.) The heat capacity shows the signature of the  $Z_2$  transition to a non-superconducting state associated with the breaking of time-reversal symmetry due to interband phase-difference locking between incoherent Cooper pairs. We consider the example of  $\beta = 4.10$ . For this inverse temperature we show a histogram of the Ising order parameter  $m$ , which clearly shows that the  $Z_2$  symmetry is broken. (The asymmetry between peaks is simply due to the finite length of the simulation.) We also illustrate the meaning of the order parameter  $m$ , which is equal to  $+1$  for one of the chiralities of the phases and equal to  $-1$  for the other chirality. **Bottom row:** Structure factors for the vorticity of  $\psi_1$  (the three components are equivalent) and the magnetic field, at the same inverse temperature  $\beta = 4.10$  as for the above histogram. Snapshots are shown to the left and thermal averages to the right. In the presence of a vortex lattice, the structure factors will have pronounced peaks. The absence of such peaks indicates that the system is in a resistive vortex-liquid state. (We remove the trivial zero-wave-vector components of the structure factors for clarity, and normalize the remaining components to the zero-wave-vector component.)

model (1) when there is an external magnetic field. Our experimental results strongly suggests that a  $Z_2$  metal phase is present even in the limit of zero magnetic field. This suggests that the cost of domain wall excitations relative to vortex excitations is underestimated by the basic model (1). The basic model relies on retaining the lowest terms in small gaps and gradients in a weak-coupling microscopic mean-field expansion and subsequently including fluctuations. In other words, it implicitly rests on the assumption of mean-field theory weakly modified by fluctuations. The results indicate that instead more terms should be retained and that effects of strong correlations may be important in this material. For example, a disparity of the phase-sum and phase-difference stiffnesses appears when there are sufficiently strong mixed-gradient terms that lead to splitting of the phase transitions in this kind of model [31]. These terms are caused by Fermi-liquid corrections or strong correlations. While it has been argued that these terms should be expected to be strong in triplet superconductors [32], and have been calculated for superconducting states in neutron stars [33] and ultracold atoms [34], these were not microscopically derived or assessed for multiband superconductors. More detailed experimental investigation in the limit of completely shielded fields can provide more accurate constraints on the Ginzburg-Landau model, and thus yield experimental insights into the microscopic physics of the material.

While the minimal model (1) underestimates the domain-wall energy and thus the presence of the  $Z_2$  phase in zero field, nonetheless our calculations show that it supports the presence of the bosonic  $Z_2$ -metal phase in non-zero magnetic field. These calculations confirm that there is a specific-heat signature at the  $Z_2$  phase transition inside the vortex liquid state (Fig. 5). The presence of a bosonic  $Z_2$ -metal phase for the model we consider is illustrated by Fig. 5. In the middle row we show a histogram of the Ising order parameter for the inverse temperature  $\beta = 4.10$  that we considered. This histogram clearly shows that time-reversal symmetry is broken. In the bottom row we show structure factors for the vorticity of  $\psi_1$  (the three components are equivalent) and the magnetic field, at the same inverse temperature  $\beta = 4.10$  as for the aforementioned histogram. Both snapshots and thermal averages of the structure factors are shown. In the presence of a vortex lattice, the structure factors will have pronounced peaks. No such peaks can be seen. This demonstrates that the system is in a resistive vortex-liquid state where the superconducting phase is disordered, and yet there is a well defined Ising-type order parameter describing spontaneously broken time-reversal symmetry associated with the phase differences between bands.

The obtained theoretical result is in qualitative agreement with the experimental magnetic phase

diagram shown in Fig. 4e and 4f. The dome of  $Z_2$  metal phase expands strongly with applied field, showing that the BTRS state in fact is more robust in magnetic field compared to bulk superconductivity. This theoretical analysis and the experimental data also provide long sought-after thermodynamic evidence for the BTRS state in the superconductor  $\text{Ba}_{1-x}\text{K}_x\text{Fe}_2\text{As}_2$ . The recent experimental discovery of the BTRS state was made using the  $\mu\text{SR}$  technique, which is a local probe that cannot directly assess the BTRS order parameter or symmetry of the system. Here, we reported a splitting of the dominant specific-heat feature from the resistive phase transition while retaining its sharpness, and observed that the position of the specific-heat jump has substantially weaker external-field dependence than the position of the resistive transition. These features require a superconducting state with several broken symmetries. The effect takes place exactly where the  $\mu\text{SR}$  probe indicated the breaking of time-reversal symmetry thereby identifying the extra symmetry as  $Z_2$ .

### Conclusion

In an ordinary superconductor beyond mean-field approximation the phase transition to the normal state is described by proliferation of vortex loops or vortex lattice melting [9–11]. In that picture, there are either preformed Cooper pairs [5–7] or precursor pairing fluctuations [4] above the critical temperature. Therefore, the normal state just above the superconducting transition in ordinary materials has bosonic pairing correlations, which gradually disappear when the temperature is increased. The situation is fundamentally different for superconducting states that break time-reversal symmetry. Beyond mean-field approximation these can have two phase transitions. A novel state might appear above the superconducting phase transition in zero field or in a vortex liquid state, where the superconducting phase is disordered but the phase differences between bands have nontrivial values different from 0 or  $\pi$ . This is a novel metallic state that spontaneously breaks time-reversal symmetry. It is distinguished by an Ising-type  $Z_2$  order parameter, which describes order in interband phase differences. In contrast to the conventional mechanisms for time-reversal symmetry breaking due to magnetism, here the time-reversal symmetry breaking originates purely from momentum space, i.e. from interband Josephson currents. Therefore, the novel state is a resistive metallic state that has preformed Cooper pairs and persistent interband Josephson currents. The two  $Z_2$  states correspond to two different Josephson-current loops in momentum space: either from the first component to the second, from the second to the third and from the third back to

the first, or in the opposite order. As the application of time-reversal inverts these current loops in momentum space, the novel state represents a bosonic metal with broken  $Z_2$  symmetry.

### Acknowledgments

The work was supported by DFG (GR 4667, CA 1931/1-1 (F.C.), GRK 1621, SFB 1143 (project-id: 247310070), and the Würzburg-Dresden Cluster of Excellence on Complexity and Topology in Quantum Matter–*ct.qmat* (EXC 2147, Project ID 390858490) and the Swedish Research Council Grants No. 642-2013-7837, 2016-06122, 2016-04516, 2018-03659 and by the Göran Gustafsson Foundation for Research in Natural Sciences and Medicine. This work was performed in part at the Aspen Center for Physics, which is supported by National Science Foundation grant PHY-1607611. The simulations were performed on resources provided by the Swedish National Infrastructure for Computing (SNIC) at the National Supercomputer Center at Linköping, Sweden. This work was supported by a Grant-in-Aid for Scientific Research on Innovative Areas "Quantum Liquid Crystals" (JP19H05823) from JSPS of Japan. This work has further been supported by the European Research Council (ERC) under the European Union's Horizon 2020 research and innovation programme (Grant Agreement No. 647276-MARS-ERC-2014-CoG). Also, we acknowledge support of the HLD at HZDR, member of the European Magnetic Field Laboratory (EMFL). We acknowledge fruitful discussion with S.-L. Drechsler, D. Efremov, C. Hicks, H. Luetkens, Y. Ovchinnikov and P. Volkov. We are thankful to K. Nenkov and C. Klausnitzer for technical support.

### SUPPLEMENTARY MATERIAL

**In the supplementary material we demonstrate that one has to be very careful in the sample selection in order to obtain crystals with  $T_c^{Z_2} > T_c^{U(1)}$ . In addition, we show AC susceptibility data in magnetic field, and provide details of the determination of  $T_c^{U(1)}$  and  $T^*$  values. We also provide details of the calculations within Josephson-coupled three-component Ginzburg-Landau theory presented in the main text.**

## EXPERIMENTAL

DC susceptibility measurements were performed using a commercial superconducting quantum interference device (SQUID) magnetometer from Quantum Design. The specific heat down to 0.4 K, electrical transport, and AC susceptibility in magnetic field up to 14 T were measured in a Quantum Design physical property measurement system (PPMS).  $^{75}\text{As}$ -NQR experiments were performed using a Tecmag spectrometer in zero magnetic field. RF excitation pulses were applied in the crystallographic  $ab$ -plane using a small coil wound around the sample with  $x = 0.8$  and the mass of 0.3 mg.

### Samples

Phase purity and crystalline quality of the plate-like  $\text{Ba}_{1-x}\text{K}_x\text{Fe}_2\text{As}_2$  single crystals were examined by X-ray diffraction (XRD), and transmission electron microscopy (TEM). The  $c$ -lattice parameters were calculated from the XRD data using the Nelson Riley function. The K doping level  $x$  of the single crystals was determined using the relation between the  $c$ -axis lattice parameter and the K doping obtained in previous studies [24]. The selected single-phase samples had a mass  $\sim 0.3 - 1$  mg with a thickness  $\sim 10 - 50$   $\mu\text{m}$  and a surface area of several  $\text{mm}^2$ .

### Characterization of samples

It is a very challenging problem to grow homogeneous crystals in the doping range of interest. The usual problem is that several plate-like single crystals with a similar doping level are grown together face-to-face. To obtain a single-phase sample, we cleaved the crystals with sticky tape. This procedure is demonstrated in Fig. S1. We found that the critical temperature  $T_c^{Z_2}$  is very sensitive to the sample conditions. For the single-phase sample with  $x = 0.8$ , the anomaly in the specific heat is observed at a higher temperature as compared with the initial double-phase sample. At the same time  $T_c^{\text{U}(1)}$  is nearly unaffected by the cleavage. The shift of  $T_c^{Z_2}$  is presumably caused by the strain which appears between two glued plate-like crystals (Fig. S1d). As can be seen in Fig. 2 i of the main text, the BTRS dome in the phase diagram is very narrow in contrast to the nearly flat  $T_c^{\text{U}(1)}$ . Therefore, it appears that  $T_c^{Z_2}$  may be rather sensitive to the strain. The obtained



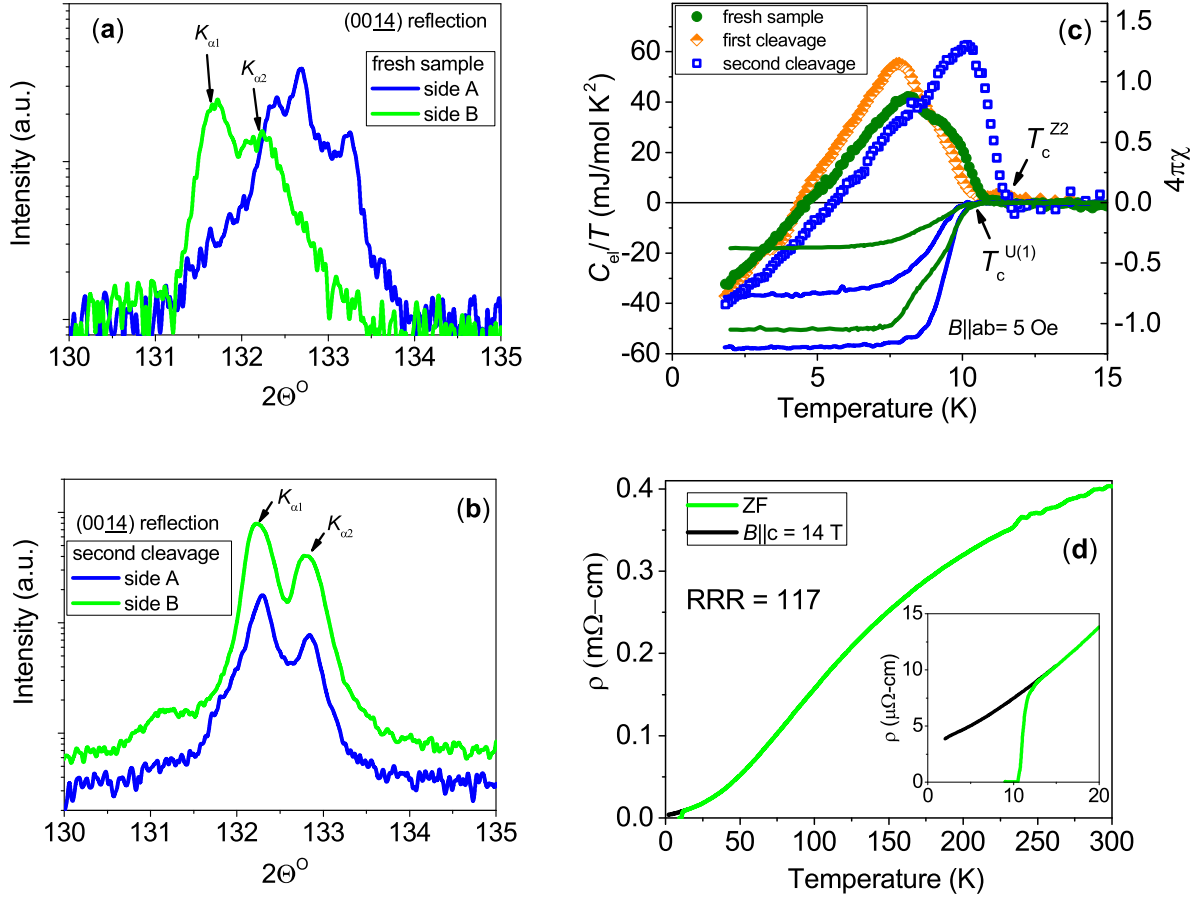


FIG. S1: **Preparation of the sample with  $x = 0.8$ .** (a) X-ray scans measured from both sides of the plate-like fresh sample, just selected from a batch ( $m_s = 1.1 \text{ mg}$ ). The position of high-angle reflections is not the same for two sample sides corresponding to two slightly different doping levels. (b) X-ray scans measured from both sides of the plate-like sample after second cleavage ( $m_s = 0.3 \text{ mg}$ ). The position of high-angle reflections is the same for two sample sides corresponding to the doping level  $x = 0.8$ . (c) Temperature dependence of the specific heat (left axis) and the DC susceptibility (right axis) of the fresh sample and after first and second cleavage.  $T_c^{U(1)}$  is nearly unaffected by the cleavage but  $T_c^{Z2}$  is clearly split off from  $T_c^{U(1)}$  after the second cleavage. Temperature dependence of the electrical resistivity of the sample after the second cleavage measured in a broad temperature range. The inset shows the data at low temperatures.

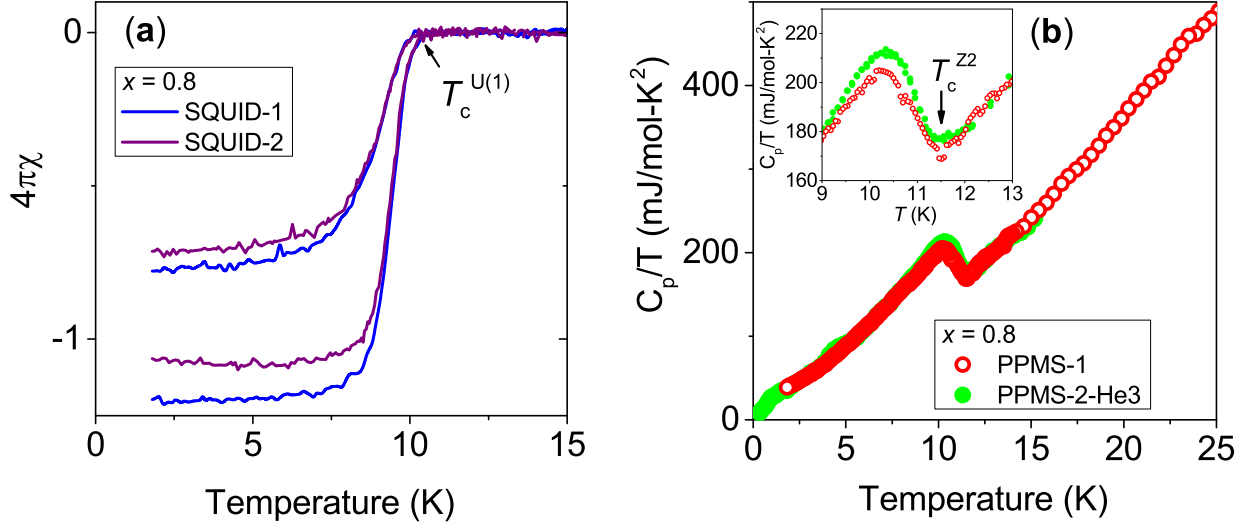


FIG. S2: **Reproducibility of the data for the sample with  $x = 0.8$**  (the data were collected after the second cleavage; see Fig. S1). (a) Temperature dependence of the DC susceptibility measured in two different SQUID magnetometers. (b) Temperature dependence of the specific heat measured in two different PPMS machines. The inset shows the data close to  $T_c^{Z2}$ .

single-phase samples had a high residual resistivity ratio  $RRR = \frac{\rho_{300K}}{\rho_0}$  as shown in Fig. S1c and in the supplementary material of Ref. [23].

We also took special care to exclude any experimental error in the measurements of the transition temperatures. The sample with  $x = 0.8$  showing the largest splitting between  $T_c^{Z2}$  and  $T_c^{U(1)}$  was remeasured several times using different PPMS and SQUIDS devices. As shown in Fig. S2 the result was essentially the same. Therefore, we exclude any possibility of experimental error in the temperature measurements.

### Criteria for $T_c^{U(1)}$ and $T^*$

In the main text we mentioned that the crossover temperature  $T^*$  for pairing fluctuations was defined from deviation of the magnetoresistance from the normal-state behaviour (see Fig. 4d). In Fig. S3a we show examples of the first derivative of the magnetoresistance at constant temperature. One can see that  $T^*$  corresponds to the sharp change in  $d\rho_{xx}(B)/dB$ . To exclude the contribution of the transversal voltage component to the magnetoresistance we also performed Hall effect measurements. The field dependencies of the Hall voltage in the normal state defined as

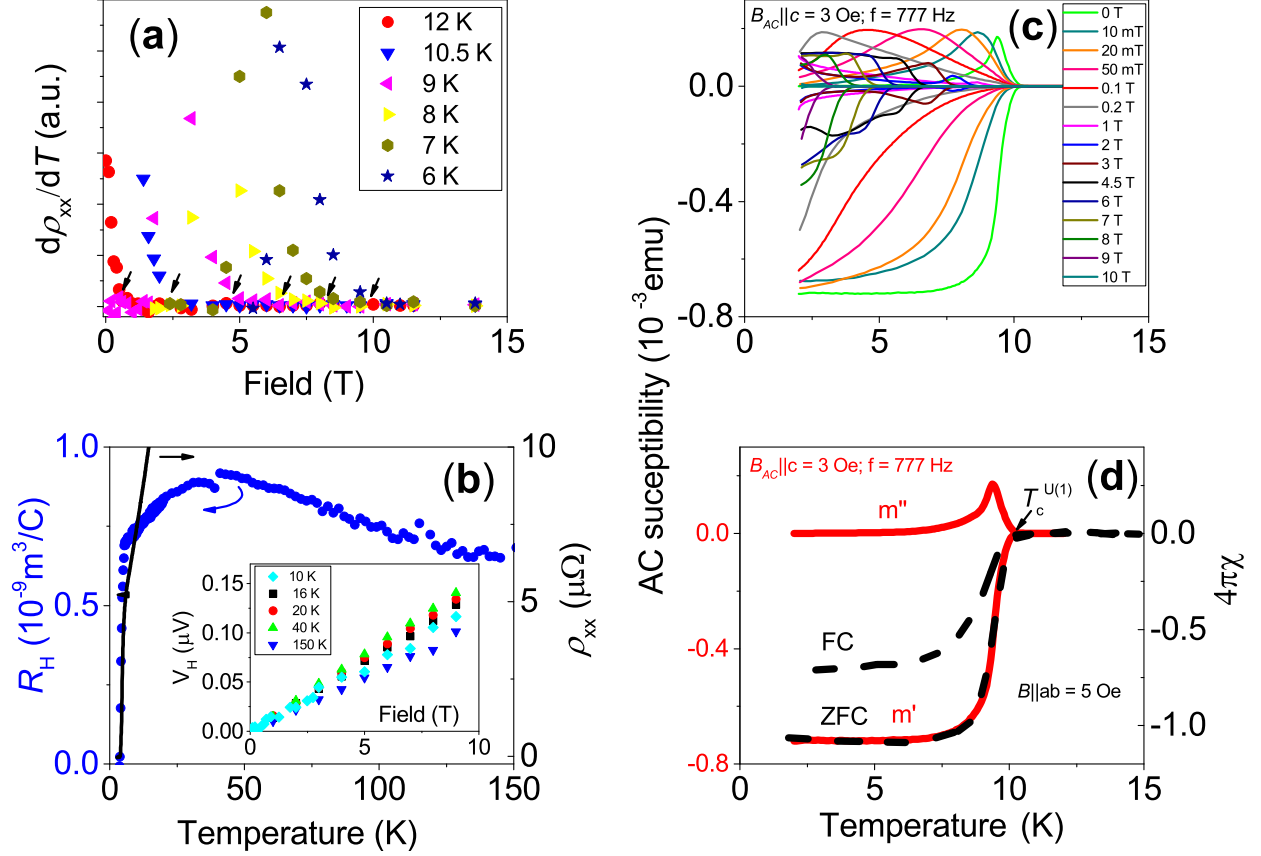


FIG. S3:  $T_c^{U(1)}$  and  $T^*$  for the sample with  $x = 0.8$  (a) Field dependence of the first derivative of the magnetoresistance  $d\rho_{xx}(B)/dB$  measured at different temperatures. (b) Temperature dependence of the Hall coefficient (left axis) and the resistivity (right axis) measured in  $B = 9$  T applied along the crystallographic  $c$ -axis. Inset shows examples of field dependencies of the Hall voltage  $V_{xy}$  in the normal state. (c) Temperature dependence of the AC susceptibility measured with AC excitation field  $B = 0.3$  mT and  $f = 777$  Hz in different DC fields applied along the crystallographic  $c$ -axis. (d) Temperature dependence of the AC susceptibility measured with AC excitation field  $B = 0.3$  mT and  $f = 777$  Hz in zero DC field (left axis), and the DC susceptibility in  $B = 5$  Oe applied in the  $ab$ -plane (right axis).

$V_H(B) = (V(B) - V(-B))/2$  in the magnetic field applied along the  $c$ -axis are shown in the inset of Fig. S3b. In the normal state  $V_H$  is linear with magnetic field in contrast to quadratic normal state magnetoresistance shown in the inset of Fig. 4d in the main text. The resulting temperature dependence of the Hall coefficient  $R_H$  is shown in Fig. S3b. The qualitatively different field dependence of  $V_H$  excludes any noticeable Hall contribution to the measured magnetoresistance in the normal state. Below  $T^*$  magnetoresistance increases while  $R_H$  reduces indicating that the linear in field dependence of the magnetoresistance below  $T^*$  cannot be caused by the Hall contribution. The overall temperature and the value of  $R_H$  is consistent with previous measurements on the

samples with similar doping range [35].

To define the bulk superconducting transition temperature  $T_c^{U(1)}$  in magnetic field, in addition to the transport data (shown in Fig. 4d), we measured the AC susceptibility in different magnetic fields (Fig. S3c).  $T_c^{U(1)}$  was defined as a temperature at which the real ( $m'$ ) and the imaginary ( $m''$ ) parts of the AC susceptibility split. We found that the  $T_c^{U(1)}$  values obtained at low frequency correspond to the onset of diamagnetic response in the DC susceptibility at low fields (Fig. S3d) and to  $T_c^{U(1)}$  defined from linear extrapolation of the field dependent resistivity in a flux-flow regime (as shown in Fig. 4d). The  $T_c^{U(1)}$  values obtained using different criteria are summarized in Figs. 4e and 4f in the main text.

## THEORY

The simulations are performed using the Metropolis-Hastings algorithm with local updates of each of the degrees of freedom. We also use parallel-tempering swaps between systems with neighboring temperatures; typically one set of swaps is proposed every 16 sweeps. The sizes of the local updates are adjusted during the equilibration in order to make the acceptance probability for each type of local update 50%. Also, the simulated temperatures are adjusted within a fixed interval in order to make the acceptance ratios for parallel-tempering swaps equal for all pairs of neighboring temperatures.

### Most favorable conditions for the formation of the $Z_2$ -metal phase in the minimal Ginzburg-Landau model of a three-band superconductor

The experiment suggests that the  $Z_2$ -metal phase occurs only in a narrow range of temperatures and only close to the top of the dome of the  $s + is$  phase. This suggests that to describe this transition one should study fluctuations in the Ginzburg-Landau, rather than London, model. Currently there is insufficient knowledge of the microscopic physics of the material to derive a precise form of the Ginzburg-Landau theory. However, one can use the experiments to constrain the commonly used class of minimal Ginzburg-Landau models

$$f = \frac{1}{2}(\nabla \times \mathbf{A})^2 + \sum_i \frac{1}{2}|(\nabla + ie\mathbf{A})\psi_i|^2 + a_i|\psi_i|^2 + \frac{b_i}{2}|\psi_i|^4 + \sum_{i<j} \eta_{ij}|\psi_i||\psi_j| \cos(\phi_i - \phi_j). \quad (\text{S1})$$

First let us assess whether the model has the  $Z_2$ -metal phase in zero magnetic field, assuming that superconductor is type II close to  $T_c$ .

Consider the question of what parameter values are most favorable for the occurrence of the  $Z_2$ -metal phase in zero magnetic field in the model (S1). First, it makes sense to make the three components symmetric, since differences between components would in general make one type of domain wall energetically preferred to the other two. Thus, we choose the parameters  $a_i$ ,  $b_i$  and  $\eta_{ij}$  to be independent of  $i$  and  $j$ , i.e. to be the same for all components and pairs of components. Second, increasing the strength of the Josephson coupling can hardly decrease the relative cost of domain walls, and thus we want the parameter  $\eta$  to be large. Now, if one increases  $\eta$  by a certain factor  $k$ , and then rescales the moduli of the matter fields, the vector potential, the spatial coordinates and the free-energy density itself thus:

$$|\psi_i| \mapsto \sqrt{k}|\psi_i|, \quad \mathbf{A} \mapsto \sqrt{k}\mathbf{A}, \quad \nabla \mapsto \sqrt{k}\nabla, \quad f \mapsto f/k^2,$$

then in terms of the rescaled quantities the free-energy density will be identical to the original one, except that  $a$  is decreased by a factor of  $k$  instead of  $\eta$  being increased by the same factor. Thus, as far as the relative temperature of the phase transitions is concerned, the limit of infinite  $\eta$  is the same as the limit of zero  $a$ , which we choose to take. With  $a$  set to zero there is, taking into account the above four freedoms to rescale, only one parameter in the continuum mean-field theory, which we take to be the electric charge  $e$ , whose role is to scale the penetration depth relative to the other length scales. The other remaining parameters in the expression for the free energy are set to 1; thus, we have  $a = 0$ ,  $b = \eta = 1$ . Now, including fluctuations we also have inverse temperature  $\beta$  as a parameter, and discretizing space we have the lattice constant  $h$ . Thus the parameters we work with are the electric charge  $e$  (which parameterizes the magnetic-field penetration length), the inverse temperature  $\beta$  and the lattice constant  $h$ .

### Length scales and normal modes

Before describing the lattice model that we use for simulations, we describe another aspect of the continuum model, namely that of length scales and normal modes. In the simplest form of multicomponent Ginzburg-Landau theory, in which the matter fields interact only through their coupling to the vector potential, there will be one coherence length  $\xi_i$  for each component. In other words, a small perturbation from the ground-state value of one of the matter-field amplitudes  $|\psi_i|$

will not induce perturbations in any other degrees of freedom, and the amplitude will asymptotically recover its ground-state value exponentially in space with characteristic length scale  $\xi_i$ .

Now consider the more general case of also having Josephson coupling between the  $N$  components. If there is no time-reversal symmetry breaking, i.e. if the ground-state phase differences are all 0 or  $\pi$ , then there will be  $N$  density modes and  $N - 1$  phase (Legett) modes, each with a corresponding length scale. (The final phase mode corresponds to a gauge transformation.) However, if time-reversal symmetry is broken, the normal modes will in general not be pure density or phase modes, instead being mixed phase-density modes [14, 36].

We have calculated ground states, length scales and normal modes for the model we consider (with the aforementioned parameters) in the way described in Ref. 14. We find that the longest characteristic length scale associated with the matter fields has the value 1.20 and the shortest the value 0.48. There is a total density mode, for which all three densities vary in unison, with length scale 0.71. The magnetic penetration depth

$$\lambda = \left( e \sqrt{\sum_i |\psi_i|^2} \right)^{-1}, \quad (\text{S2})$$

where each ground state density  $|\psi_i|^2 = 0.5$ . The model is type I when the penetration depth is the shortest length scale, i.e. when  $e > 1.7$ , and type II when the penetration depth is the longest length scale, i.e. when  $e < 0.68$ .

## MONTE CARLO SIMULATION METHODS AND OBSERVABLES

In order to perform Monte Carlo simulations, we discretize the model (1) on a three-dimensional simple cubic lattice with  $L^3$  sites and lattice constant  $h$ . The discretized model is given by the free-energy density

$$f = \frac{1}{2h^2} \sum_{k < l} F_{kl}^2 - \frac{1}{h^2} \sum_{i,k} |\psi_i(\mathbf{r})| |\psi_i(\mathbf{r} + \mathbf{k})| \cos \chi_{i,k}(\mathbf{r}) + \sum_i \left( a_i + \frac{3}{h^2} \right) |\psi_i(\mathbf{r})|^2 + \frac{b_i}{2} |\psi_i(\mathbf{r})|^4 + \sum_{i < j} \eta_{ij} |\psi_i(\mathbf{r})| |\psi_j(\mathbf{r})| \cos(\phi_i - \phi_j), \quad (\text{S3})$$

where

$$F_{kl} = A_k(\mathbf{r}) + A_l(\mathbf{r} + \mathbf{k}) - A_k(\mathbf{r} + \mathbf{l}) - A_l(\mathbf{r}) \quad (\text{S4})$$

is a lattice curl,

$$\chi_{i,k}(\mathbf{r}) = \phi_i(\mathbf{r} + \mathbf{k}) - \phi_i(\mathbf{r}) + heA_k(\mathbf{r}) \quad (\text{S5})$$

is a gauge-invariant phase difference,  $k$  and  $l$  signify coordinate directions, and  $\mathbf{k}$  is a vector pointing from a lattice site to the next site in the  $k$ -direction. We use periodic boundary conditions in all three spatial directions. The thermal probability distribution for configurations of the system at inverse temperature  $\beta$  is given by the Boltzmann weight

$$e^{-\beta F}, \quad F = h^3 \sum_{\mathbf{r}} f(\mathbf{r}), \quad (\text{S6})$$

and we generate representative samples from these thermal distributions using Monte Carlo simulation.

We now describe the quantities that are measured during the simulations and the methods we use to locate phase transitions.

### Locating superconducting transitions

Superconducting transitions in zero external magnetic field can be located using the dual stiffness [37–39]

$$\rho^\mu(\mathbf{q}) = \left\langle \frac{|\sum_{\mathbf{r},\nu,\lambda} \epsilon_{\mu\nu\lambda} \Delta_\nu A_\lambda(\mathbf{r}) e^{i\mathbf{q}\cdot\mathbf{r}}|^2}{(2\pi)^2 L^3} \right\rangle, \quad (\text{S7})$$

where  $\epsilon_{\mu\nu\lambda}$  is the Levi-Civita symbol,  $\Delta_\nu$  is a difference operator and  $\langle \cdot \rangle$  is a thermal expectation value. In particular, we consider the dual stiffness in the  $z$ -direction evaluated at the smallest relevant wave vector in the  $x$ -direction  $\mathbf{q}_{\min}^x = (2\pi/L, 0, 0)$ , i.e.  $\rho^z(\mathbf{q}_{\min}^x)$ , which we denote simply as  $\rho$ . In the thermodynamic limit, this quantity is zero in the superconducting phase in which fluctuations of the magnetic field are suppressed, and non-zero in the normal phase. Thus it is a dual order parameter in the sense that it is zero in the low-temperature phase and non-zero in the high-temperature phase. At the critical point of a continuous superconducting transition, the quantity  $\rho$  is expected to scale as  $1/L$ , so that  $L\rho$  is a universal quantity. We use finite-size crossings of  $L\rho$ , extrapolated to the thermodynamic limit, in order to locate superconducting transitions.

### Locating $Z_2$ metal transitions

Time-reversal symmetry is  $Z_2$ , i.e. is described by the previously defined Ising order parameter  $m$ . In order to locate transitions to states that break time-reversal symmetry, we use the Binder cumulant for the order parameter  $m$ :

$$U = \frac{\langle m^4 \rangle}{3\langle m^2 \rangle^2}. \quad (\text{S8})$$

In the thermodynamic limit, this quantity is equal to 1 in the high-temperature phase in which the distribution function for the order parameter is given by a single Gaussian centered around  $m = 0$ , and equal to  $1/3$  in the low-temperature phase in which the distribution function is given by two separated Gaussians at  $m = \pm m_0 \neq 0$ . For a continuous transition, the distribution function for the order parameter is expected to have a universal shape at the critical point, so that the Binder cumulant  $U$  is a universal quantity. We use finite-size crossings of the Binder cumulant  $U$ , extrapolated to the thermodynamic limit, in order to locate  $Z_2$  transitions.

### External magnetic field

In order to implement external magnetic field, we write the vector potential as a sum of two terms:  $\mathbf{A}(\mathbf{r}) = \mathbf{A}_0(\mathbf{r}) + \mathbf{A}_1(\mathbf{r})$ . The first part of the vector potential corresponds to a uniform magnetic field in the  $z$  direction, implemented in the Landau gauge, and is held fixed:  $\mathbf{A}_0(\mathbf{r}) = (0, 2\pi x f, 0)$ . The second part of the vector potential,  $\mathbf{A}_1(\mathbf{r})$ , is allowed to fluctuate thermally. Due to the periodic boundary conditions imposed on  $\mathbf{A}_1(\mathbf{r})$ , the contribution to total magnetic flux from this part of the vector potential is zero, so that the total flux is constant and equal to that given by  $\mathbf{A}_0(\mathbf{r})$ . In order to be consistent with the periodic boundary conditions, the value of  $f$  must be chosen so that  $eLh^2f$  is an integer.

In order to detect the presence or absence of a vortex lattice in external magnetic field, we consider two types of quantity: vorticities (to be defined below) and magnetic flux density. For both types of quantity, we measure averages over the direction of the applied field (the  $z$  direction), thus obtaining 2D images. We also consider the absolute values of the Fourier transforms of these, which are structure factors.

The vorticity is defined as follows: For a phase field defined on continuous space, the meaning



of there being a vortex at a certain point is clear: the phase winding around this point is nonzero. For a phase field defined only on a discrete lattice the meaning of there being a vortex is less clear, and a definition that is reasonable and consistent with the continuum limit must be made. The standard way to count the number of vortices on a given plaquette is this: For each link of the plaquette, consider the gauge-invariant phase difference  $\chi_{i,k}(\mathbf{r})$ . For each multiple of  $2\pi$  that must be added (subtracted) to  $\chi_{i,k}(\mathbf{r})$  in order to bring it into the primary interval  $(-\pi, \pi]$ , add  $+1$  ( $-1$ ) to the vorticity of the plaquette.

**ASSESSING THE EXISTENCE OF THE BOSONIC  $Z_2$ -METAL PHASE IN THE  
MINIMAL GINZBURG-LANDAU MODEL IN THE TYPE II REGIME IN ZERO  
EXTERNAL FIELD**

We have performed Monte-Carlo simulations of the model we consider for various values of the electric charge  $e$  and the lattice constant  $h$ . We consider three values of the electric charge:  $e = 0.5, 1.0, 2.0$ . We note that these values correspond to the cases where the magnetic field penetration length is the largest, an intermediate or the smallest length scale, respectively. For each value of the charge, we construct a phase diagram in terms of inverse temperature  $\beta$  and lattice constant  $h$ , as shown in Fig. S4. The phase transitions are located by considering finite-size crossings of the Binder cumulant  $U$ , and of the dual stiffness  $\rho$  scaled by system size  $L$ , examples of which are also shown in Fig. S4.

Using the aforementioned phase diagrams, we estimate for which values of the charge  $e$  and the lattice constant  $h$  the anomalous fluctuation-induced bosonic  $Z_2$ -metal phase occurs. We do this by fitting second-order polynomials to the determined points on the phase diagram (Fig. S4), in order to estimate the position of the bicritical point at which the transitions merge. The result is shown in Fig. S4: the  $Z_2$ -metal phase is estimated to occur for values of  $e$  and  $h$  greater than those indicated by the purple dots, thus roughly in the purple region in the top right-hand corner (the line is a guide to the eye).

In order to assess if the material is described by the minimal version of the continuum Ginzburg-Landau model we started from, we consider the following two requirements: First, the indications are that the material is relatively strongly type II when substantially outside of the  $Z_2$  phase transition. Thus in setting up the lattice model the bare penetration length must be large enough

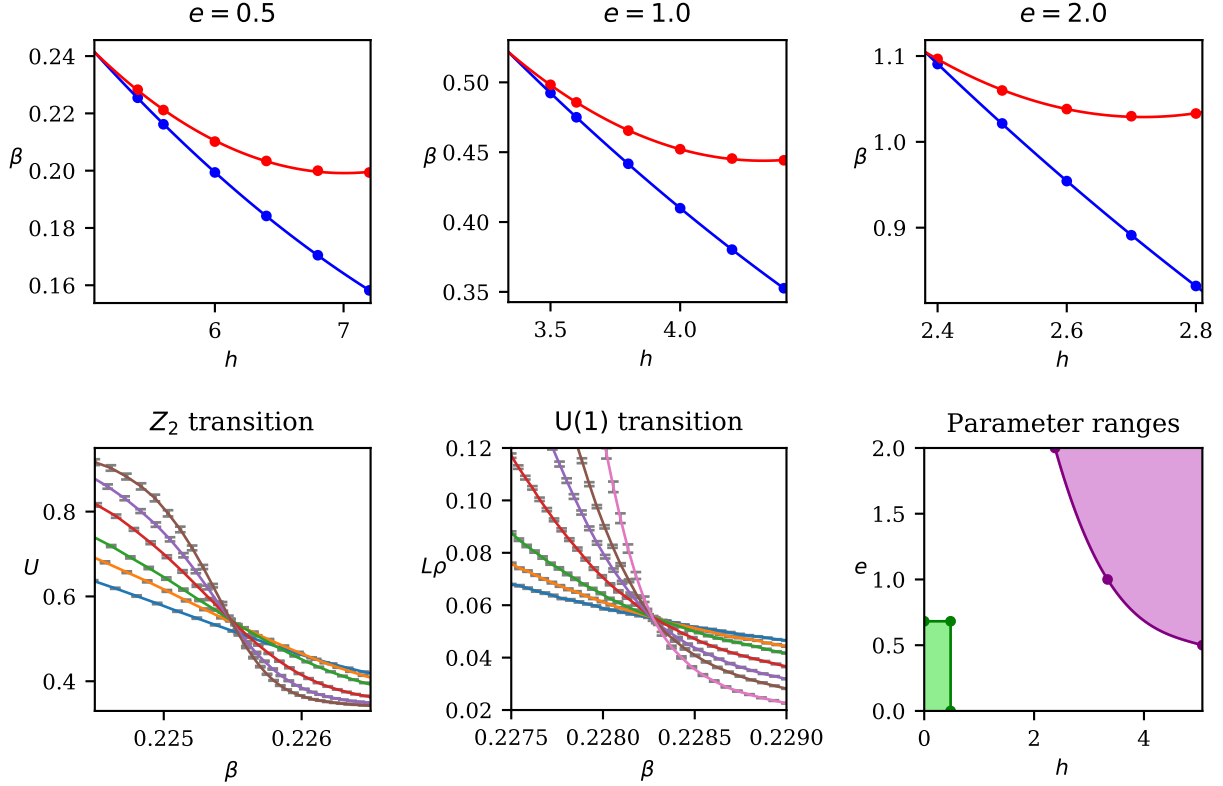


FIG. S4: **Top row:** Phase diagrams in terms of inverse temperature  $\beta$  and lattice constant  $h$  for the three charges  $e = 0.5, 1.0, 2.0$  with  $Z_2$  transitions shown in blue (bottom curves) and superconducting transitions in red (top curves). The lines are second-order polynomials fitted to the transition points; we use these lines to estimate the positions of the points where the transitions merge. Errors are smaller than symbol sizes. **Bottom row, left and center:** Examples of how the points in the above phase diagrams are determined using finite-size crossings of the Binder cumulant  $U$  and the quantity  $L\rho$ . The parameters are  $e = 0.5$ ,  $h = 5.4$  (leftmost pair of points in the above diagrams). The system sizes are  $L = 8, 10, 12, 16, 20, 24$  for the  $Z_2$  transition; for the U(1) transition  $L = 32$  is also shown. **Bottom row, right:** Regions of  $e-h$  space for which the bosonic  $Z_2$ -metal phase is estimated to occur (purple, top right; the line is a guide to the eye), and for which the system is type II and the lattice constant is the shortest length scale (green, bottom left). The two regions are well separated, which indicates that the bosonic  $Z_2$ -metal phase does not occur in the type II regime of the minimal continuum Ginzburg-Landau model we consider if the system is three-dimensional and there is no applied magnetic field.

relative to other characteristic length scales. In our dimensionless units the electric charge parameterizes the magnetic field penetration length, and thus the electric charge must be small enough. Second, the lattice constant must be smaller than the other characteristic length scales. The region of  $e$ - $h$  space for which the model is type II and the lattice constant is the shortest length scale is that shown in green in Fig. S4. The green (relevant parameters) and purple ( $Z_2$  metal) regions are well separated, which indicates that the bosonic  $Z_2$ -metal phase does not occur in the type II regime of the minimal continuum Ginzburg-Landau model in the absence of applied field. Since the experimental results indicate that the bosonic  $Z_2$ -metal phase does exist in zero field, this suggests that one of the following is true: (i) The system is not described by the minimal Ginzburg-Landau model at the doping and temperature range in question. In other words, for this system it is not the case that mean-field theory is only weakly modified by fluctuations, which would allow one to use only the lowest terms in microscopic mean-field expansions and include fluctuations in such reduced models. For example, Fermi-liquid corrections or strong correlation effects are important because they result in mixed-gradient terms, which are second order in derivatives and fourth order in fields, and which enhance the phase-difference stiffness relative to the phase-sum stiffness [31]. Thus, these terms enhance the domain-wall energy compared to the vortex energy, and thus create the bosonic  $Z_2$ -metal phase in zero field. (ii) In the fluctuation regime the correlation length becomes comparable to sample thickness, leading to a Kosterlitz-Thouless transition for which the  $Z_2$ -metal phase exists in zero field.

### BOSONIC $Z_2$ -METAL PHASE IN NON-ZERO FIELD

Although the bosonic  $Z_2$ -metal phase does not occur in the type II regime of the minimal Ginzburg-Landau model in zero external field, it does occur in non-zero field. It has previously been demonstrated that this kind of phase forms in external field because melting of the lattice of one-quanta vortices restores the  $U(1)$  symmetry but preserves the broken symmetry associated with the phase difference of the order parameters [20, 21, 30]. We demonstrate that the effect is present in the minimal Ginzburg-Landau model (S1). Specifically, we give an example of this for the charge  $e = 0.5$ , which makes the system type II, and the lattice constant  $h = 0.7$ , which is shorter than the penetration depth, the characteristic length scale of the lightest phase-density mode (that with the longest length scale) and the length scale of the total density mode (in fact, the two lightest phase-density modes are degenerate, as are the two heaviest ones.) The system

size we use is  $L = 64$ , and the applied magnetic field is the weakest non-zero field applicable in the Landau gauge for this system size with periodic boundary conditions.

---

\* Electronic address: [vadim.a.grinenko@gmail.com](mailto:vadim.a.grinenko@gmail.com)

† Electronic address: [babaev.egor@gmail.com](mailto:babaev.egor@gmail.com)

- [1] J. Bardeen, L. N. Cooper, and J. R. Schrieffer, Phys. Rev. **106**, 162 (1957).
- [2] J. Bardeen, L. N. Cooper, and J. R. Schrieffer, Phys. Rev. **108**, 1175 (1957).
- [3] V. L. Ginzburg and L. D. Landau, Zh. Eksp. Teor. Fiz. **20**, 1064 (1950).
- [4] L. Aslamazov and A. Larkin, Fizika tverdogo tela **10**, 1104 (1968).
- [5] A. J. Leggett, in *Modern trends in the theory of condensed matter* (Springer, 1980), pp. 13–27.
- [6] P. Nozieres and S. Schmitt-Rink, Journal of Low Temperature Physics **59**, 195 (1985).
- [7] V. Emery and S. Kivelson, Nature **374**, 434 (1995).
- [8] M. E. Peskin, Ann. Phys. **113**, 122 (1978), ISSN 0003-4916.
- [9] C. Dasgupta and B. I. Halperin, Phys. Rev. Lett. **47**, 1556 (1981).
- [10] D. R. Nelson, Physical review letters **60**, 1973 (1988).
- [11] D. S. Fisher, M. P. Fisher, and D. A. Huse, Physical Review B **43**, 130 (1991).
- [12] B. Svistunov, E. Babaev, and N. Prokofev, *Superfluid States of Matter* (CRC Press, 2015).
- [13] V. Stanev and Z. Tesanovic, Phys. Rev. B **81**, 134522 (2010).
- [14] J. Carlström, J. Garaud, and E. Babaev, Phys. Rev. B **84**, 134518 (2011).
- [15] S. Maiti and A. V. Chubukov, Phys. Rev. B **87**, 144511 (2013).
- [16] J. Böker, P. A. Volkov, K. B. Efetov, and I. Eremin, Phys. Rev. B **96**, 014517 (2017).
- [17] M. Silaev, J. Garaud, and E. Babaev, Physical Review B **95**, 024517 (2017).
- [18] T. A. Bojesen, E. Babaev, and A. Sudbø, Phys. Rev. B **88**, 220511 (2013).
- [19] T. A. Bojesen, E. Babaev, and A. Sudbø, Phys. Rev. B **89**, 104509 (2014).
- [20] E. Babaev, A. Sudbø, and N. Ashcroft, Nature **431**, 666 (2004).
- [21] E. Smørgrav, E. Babaev, J. Smiseth, and A. Sudbø, Phys. Rev. Lett. **95**, 135301 (2005).
- [22] V. Grinenko, P. Materne, R. Sarkar, H. Luetkens, K. Kihou, C. H. Lee, S. Akhmadaliev, D. V. Efremov, S.-L. Drechsler, and H.-H. Klauss, Phys. Rev. B **95**, 214511 (2017).
- [23] V. Grinenko, R. Sarkar, K. Kihou, C. H. Lee, I. Morozov, S. Aswartham, B. Büchner, P. Chekhonin, W. Skrotzki, K. Nenkov, et al., Nat. Phys. **16**, 789–794 (2020).
- [24] K. Kihou, T. Saito, K. Fujita, S. Ishida, M. Nakajima, K. Horigane, H. Fukazawa, Y. Kohori, S.-i. Uchida, J. Akimitsu, et al., Journal of the Physical Society of Japan **85**, 034718 (2016), <https://doi.org/10.7566/JPSJ.85.034718>.
- [25] A. Chubukov, *Itinerant Electron Scenario* (Springer International Publishing, Cham, 2015), pp. 255–329, ISBN 978-3-319-11254-1.

- [26] J. Garaud, J. Carlström, and E. Babaev, *Phys. Rev. Lett.* **107**, 197001 (2011).
- [27] J. Garaud, J. Carlström, E. Babaev, and M. Speight, *Phys. Rev. B* **87**, 014507 (2013).
- [28] G. Blatter, M. V. Feigel'man, V. B. Geshkenbein, A. I. Larkin, and V. M. Vinokur, *Rev. Mod. Phys.* **66**, 1125 (1994).
- [29] J. Garaud, M. Silaev, and E. Babaev, *Physica C* **533**, 63 (2017), ISSN 0921-4534, ninth international conference on Vortex Matter in nanostructured Superconductors.
- [30] T. A. Bojesen and A. Sudbø, *Phys. Rev. B* **90**, 134512 (2014).
- [31] E. V. Herland, E. Babaev, and A. Sudbø, *Phys. Rev. B* **82**, 134511 (2010).
- [32] A. J. Leggett, *Reviews of Modern Physics* **47**, 331 (1975).
- [33] O. Sjöberg, *Nuclear Physics A* **265**, 511 (1976), ISSN 0375-9474.
- [34] K. Sellin and E. Babaev, *Phys. Rev. B* **97**, 094517 (2018).
- [35] Y. Liu and T. A. Lograsso, *Phys. Rev. B* **90**, 224508 (2014).
- [36] J. Garaud, A. Corticelli, M. Silaev, and E. Babaev, *Physical Review B* **98**, 014520 (2018).
- [37] O. I. Motrunich and A. Vishwanath, *arXiv* (2008), 0805.1494v1.
- [38] E. V. Herland, T. A. Bojesen, E. Babaev, and A. Sudbø, *Phys. Rev. B* **87**, 134503 (2013).
- [39] J. Carlström and E. Babaev, *Phys. Rev. B* **91**, 140504 (2015).